

## Analysis of single particle and collective beam effects in high intensity beams in a periodic quadrupole channel

Rajni Pande<sup>1</sup>,<sup>✉</sup> Monika Phogat,<sup>1</sup> and Srinivas Krishnagopal<sup>2</sup>

<sup>1</sup>*Ion Accelerator Development Division, Bhabha Atomic Research Centre, Mumbai-400085, India*

<sup>2</sup>*Homi Bhabha National Institute, Mumbai-400094, India*

 (Received 5 September 2023; accepted 20 February 2024; published 19 March 2024)

In high intensity proton accelerators, there are two main mechanisms that can cause beam degradation: incoherent and coherent effects due to nonlinear space charge forces. The incoherent effects represent the single particle dynamics while the coherent effects represent the collective response of the beam. Of particular interest is the region above a zero current phase advance ( $\sigma_0$ ) of  $90^\circ$  where the (coherent) second-order envelope instability and the (incoherent) fourth-order particle resonance are seen to lead to emittance growth. Large emittance growth is also seen below the envelope instability region as the full current beam phase advance ( $\sigma$ ) decreases. In the present study, we have studied the nonlinear effects in a high intensity beam propagating through a focusing-defocusing (FD) quadrupole channel for  $\sigma_0$  greater than  $90^\circ$ , both analytically, by studying the solutions of Kapchinsky-Vladimirsky (KV) equation and the particle core model, and through detailed particle-in-cell (PIC) simulations using the TRACEWIN code. The KV envelope equation gives the collective response of the beam while the particle core model gives the contribution of the single particle effects. With pic simulations, which resemble the behavior of the real beams more closely as compared to envelope calculations or the particle core model, it is possible to study the evolution of the beam in a self-consistent manner. Our studies show, that it is possible to identify the specific process responsible for beam degradation in high intensity beams. It is also possible to identify which process dominates under different conditions. We further show that the width of the emittance increase stop band calculated from PIC simulations is wider than that calculated by the envelope equations and that the width depends on the length of the channel being studied.

DOI: [10.1103/PhysRevAccelBeams.27.034201](https://doi.org/10.1103/PhysRevAccelBeams.27.034201)

### I. INTRODUCTION

In recent years, there has been a lot of interest in the development of high intensity proton accelerators for applications like Accelerator Driven Systems (ADS) [1–5], Spallation Neutron Sources (SNS) [6–8], Radioactive Ion Beam (RIB) production [9], Neutrino factories [10], etc. These accelerators are required to operate at high beam currents of the order of milli amperes for various applications. At these currents, the nonlinear space charge forces are very high and can lead to an increase in beam emittance and the formation of beam halos. The main design goal in high intensity accelerators, in order to allow hands-on maintenance, is to minimize the beam loss by avoiding or minimizing contributions of various halo-forming mechanisms. There are several mechanisms that can cause significant halo formation and lead to beam loss. Among these are

coherent and incoherent effects due to the nonlinear space charge forces of the high intensity beam. The coherent effects are due to the dynamics of the beam as a whole while incoherent effects are due to the dynamics of single particles in the beam. These can lead to beam degradation causing an increase in beam size, beam emittance, and halo formation.

The second-order envelope instability [11–15], which is a coherent effect, and the fourth-order single particle resonance [16,17], which is a single particle effect, have been widely studied in the past. These effects have also been widely studied in circular accelerators [18–22]. All linear accelerators were designed to avoid the envelope instability by keeping the zero current phase advance ( $\sigma_0$ ) less than  $90^\circ$ . The earliest experimental study in a periodic focusing-defocusing (FD) channel, done by Tiefenback using 87 quadrupoles, showed beam degradation when  $\sigma_0$  was greater than  $90^\circ$ . However, the beam behavior was not consistent with the calculated envelope instability stop band [23,24]. Several experiments were also done at UNILAC at GSI to study the variation of beam emittance with phase advance [25,26]. In 2009, experiments conducted at UNILAC at GSI revealed that for  $\sigma_0 > 90^\circ$ , the fourth-order particle resonance is excited [26]. Another experiment at the Spallation Neutron Source (SNS) at

---

*Published by the American Physical Society under the terms of the Creative Commons Attribution 4.0 International license. Further distribution of this work must maintain attribution to the author(s) and the published article's title, journal citation, and DOI.*

Oakridge also confirmed the presence of the fourth-order particle resonance [27]. Compact linear Paul trap devices have also been used to study, experimentally and theoretically, coherent and incoherent resonances in periodic focusing channels [28]. There has been much debate on whether the envelope instability or the fourth-order resonance dominates for  $\sigma_0 > 90^\circ$ . Several studies have tried to distinguish between these two effects [29–32]. High emittance growth is also seen below the envelope instability region as the full current beam phase advance decreases. In this paper, we study the differences between the two processes and identify the specific process responsible for beam degradation under different initial conditions, for  $\sigma_0 > 90^\circ$ .

In the transport of real beams with space charge through periodic focusing channels, both, coherent and incoherent, effects are responsible for the increase in beam emittance and beam halo formation. The coherent effects are the collective behavior of the beam as a whole. These are excited by beam mismatch and can lead to resonances [33,34] and instabilities [13] of the beam envelope. The second-order envelope instability is a well-known collective effect of the beam as a whole for  $\sigma_0 > 90^\circ$  and is responsible for accelerator designers keeping the zero current phase advance  $\sigma_0$  less than  $90^\circ$ . It is possible to study the coherent effects of the beam envelope by analytical calculations using the Kapchinsky-Vladimirsky (KV) envelope equations. These were first derived, for a continuous beam with uniform charge density and elliptical cross section, by Kapchinsky and Vladimirsky [35]. Later, Sacherer showed that the linear part of the self-field depends mainly on the rms size of the distribution and only weakly on its exact form [36]. Since then, the KV envelope equation has been used extensively to study the beam collective instability [11,12], nonlinear dynamics of beam envelope [33,34], and beam halo formation. The perturbed KV envelope equations of motion around the matched beam envelopes can be utilized to analyze the stability properties of the beam envelope by calculating the eigenvalues of the transfer map over one lattice period. These effects can also be studied through envelope tracking calculations that use matrix multiplication and consider a linear space charge due to a uniform beam, as in envelope tracking codes.

The incoherent effects represent the single particle behavior of the beam and can be seen as single particle resonances. The single particle resonances are excited when the resonance condition

$$mk_{xy} = 360^\circ$$

is satisfied. Here,  $m$  is the order of the resonance and  $k_{xy}$  is the single particle phase advance per focusing lattice period. Of particular interest is the fourth-order particle



FIG. 1. The quadrupole FD lattice used for the study.

resonance for  $m = 4$ , which is seen for high current beams in a lattice with  $\sigma_0 > 90^\circ$ .

Since both, the second-order envelope instability and the fourth-order particle resonance, are seen for  $\sigma_0 > 90^\circ$ , and both cause an increase in beam emittance and lead to beam halo formation, it is important to differentiate between the two processes and identify when one process dominates over the other. In the present work, we have studied the collective behavior of the beam by studying the behavior of the beam envelope for various initial conditions using the analytical envelope equation. The collective beam behavior has also been studied using the envelope tracking matrix method using the TRACEWIN [37] code. In addition, the tools of nonlinear analysis like Poincare maps and fixed point analysis [38] have also been used to study the collective instability. The single particle behavior has been studied in a simple way using the particle core model [39–43]. Then, the overall behavior of the beam was studied by performing self-consistent PIC simulations using TRACEWIN.

For all studies, a proton beam of energy 150 keV propagating in a periodic focusing-defocusing (FD) quadrupole lattice has been considered [12]. The length of the period of the lattice is 0.2 m and the length of the quadrupole lenses is 0.1 m as shown in Fig. 1.

## II. SECOND-ORDER BEAM ENVELOPE INSTABILITY

An intense particle beam propagating in a periodic focusing channel in the presence of mismatch will experience nonlinear resonances, collective instability, or chaotic motion depending on the values of  $\sigma_0$  and  $\sigma$ . Here  $\sigma_0$  is the zero current phase advance per focusing period and  $\sigma$  is the phase advance per period of the beam with current, i.e., in the presence of space charge. A smaller value of  $\sigma$  denotes a larger beam current. A widely studied phenomenon is the second-order envelope instability which can result in significant beam degradation. The envelope instability can be studied analytically by solving the KV envelope equation with mismatch and finding the stability of the eigenvalues [11].

The transverse KV envelope equations can be written as

$$\frac{d^2 X}{ds^2} - k_x(s)X - \frac{K}{X+Y} - \frac{\epsilon_x^2}{X^3} = 0, \quad (1)$$

$$\frac{d^2 Y}{ds^2} + k_y(s)Y - \frac{K}{X+Y} - \frac{\epsilon_y^2}{Y^3} = 0, \quad (2)$$

where  $X$  and  $Y$  denote the rms beam size in  $x$  and  $y$ , respectively,  $\varepsilon_x$  and  $\varepsilon_y$  are the beam emittance in  $x$  and  $y$ , respectively,  $k_x$  and  $k_y$  measure the strength of the applied periodic FD magnetic field and  $K = 2qI/4\pi\epsilon_0 mc^3\beta^3\gamma^3$  is the generalized perveance of the beam which is a measure of the beam space charge [11,32].

For a quadrupole channel,

$$k_x(s) = -k_y(s) = k(s) = \frac{G}{mc\beta\gamma},$$

where  $G$  is the quadrupole gradient.

For a periodic lattice with periodicity  $L$ , the zero current phase advance over one period can be defined as

$$\sigma_0 = \left( L \int_0^L k(s) ds \right)^{1/2}.$$

The beam phase advance for a matched beam in the periodic channel can be defined as

$$\sigma_x = \int_s^{s+L} \frac{\varepsilon_x}{X^2} ds \quad \text{and} \quad \sigma_y = \int_s^{s+L} \frac{\varepsilon_y}{Y^2} ds.$$

For the lattice shown in Fig. 1, a stability analysis using the KV envelope Eqs. (1) and (2) indicates that the envelope instability exists for  $\sigma_0 > 90^\circ$  for a range of  $\sigma$  values, as can be seen in Fig. 2. The orange line represents the upper bound of the instability while the blue line represents the lower bound. We see that as  $\sigma_0$  is increased above  $90^\circ$ , for each value of  $\sigma_0$ , there is a range of values of  $\sigma$  for which the envelope instability is excited. The region between the upper and lower bounds of the instability is known as the instability stop band. The width of the stop band corresponding to the envelope instability increases with the increasing value of  $\sigma_0$ .

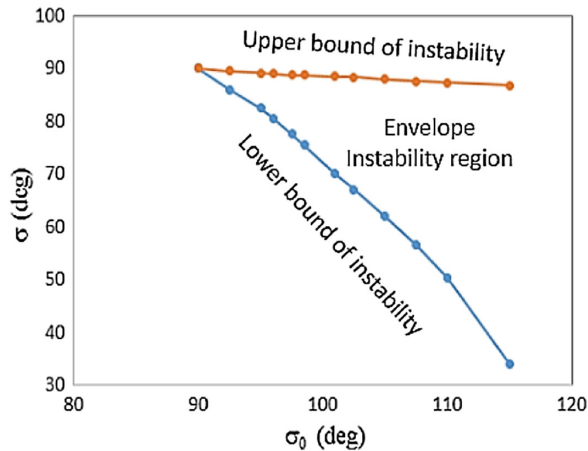


FIG. 2. Envelope instability stop bands for the FD lattice shown in Fig. 1.

A beam or an envelope is said to be matched if the values of  $X$  and  $Y$  and  $X'$  and  $Y'$  remain the same after the completion of one lattice period. The solutions of Eqs. (1) and (2) provide the matched beam solutions. Equations (1) and (2) are coupled and can be solved for different values of the space charge parameter ( $K$ ), chosen such that the beam phase advance lies outside and within the instability region. The phase space analysis of these equations has been studied analytically using Poincare maps [38]. The Poincare map preserves many properties of the periodic and quasiperiodic orbits of the original system. It has a lower dimensionality than the original phase space and can therefore be used for analyzing the system in a simpler way. For a matched beam of period 1, the envelope intersects the Poincare surface of the section at the same point after every lattice period which is seen as a fixed point. This can be seen in Figs. 3(a) and 3(b) for beam phase advance lying outside the envelope instability region ( $\sigma_0 = 100^\circ$  and  $\sigma = 89^\circ$ ). In the envelope instability stop band, the beam does not remain matched and hence the envelope will not intersect at the same point in the Poincare section as seen in Figs. 3(a) and 3(b) ( $\sigma_0 = 100^\circ$  and  $\sigma = 73^\circ$ ). Since the

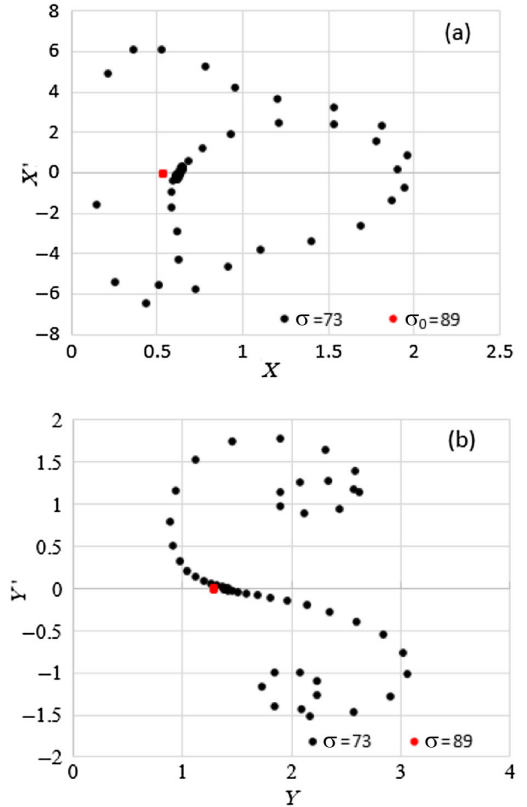


FIG. 3. Poincare surface of section in  $X$  and  $Y$  phase space for 50 FD periods, for  $\sigma_0 = 100^\circ$ , in different regions (a) in  $X$ - $X'$  phase space for  $\sigma = 89^\circ$  which lies in the envelope stable region with a fixed point in the phase space and for  $\sigma = 73^\circ$  which lies in the envelope instability region. No stable fixed point is seen in the envelope instability region. (b) in  $Y$ - $Y'$  phase space.

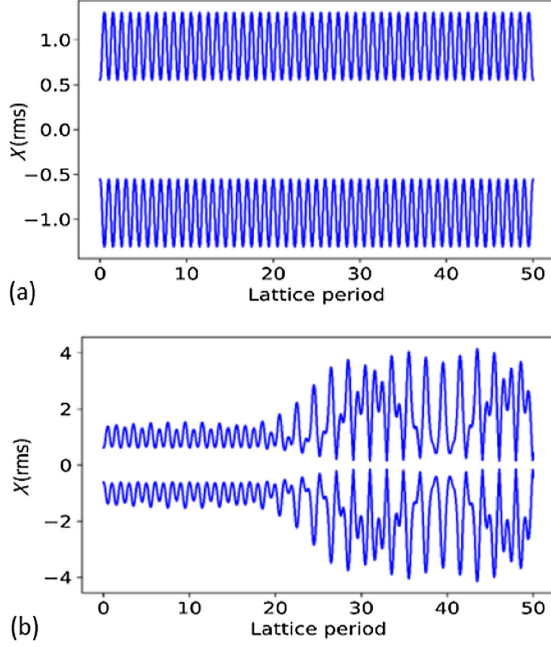


FIG. 4. Beam envelope in  $X$  (similar behavior is observed for the  $Y$  envelope) for (a) the stable region ( $\sigma_0 = 100^\circ$ ,  $\sigma = 89^\circ$ ) and (b) the unstable region ( $\sigma_0 = 100^\circ$ ,  $\sigma = 73^\circ$ ), calculated from the solution of the KV envelope equation.

envelope instability is a parametric resonance of second order, envelope intersection in the Poincare section is expected to be a bifurcation of the fixed point into two islands [as in Figs. 3(a) and 3(b) for  $\sigma = 73^\circ$ ]. For the first 50 lattice periods, the Poincare section shows two resonance islands in  $Y$ - $Y'$ . For an FD channel, due to the coupling between  $X$  and  $Y$ , bifurcation in  $X$ - $X'$  is not very clear. It can be seen that the beam remains matched outside the instability stop band. In the envelope instability region, since no matched beam exists, it is characterized by the absence of a stable fixed point in the Poincare map [44]. The corresponding matched beam envelope for the stable region and instability region are shown in Figs. 4(a) and 4(b). The envelope instability is characterized by an erratic change in the beam envelope. Studies using the Poincare map show that there exists a fixed point for all values of  $(\sigma_0, \sigma)$  except in the envelope instability stop band.

The envelope instability can also be studied by envelope calculations using matrix multiplication, where the space charge is included as a linear defocusing force using TRACEWIN. The envelope instability grows exponentially from an infinitesimal mismatch up to saturation [29]. We define  $\Delta a/a$ , the maxima of relative growth in the beam size taken over the 206 periods, as the strength of the instability. Figure 5 shows the variation of the strength of the instability for different values of  $\sigma_0$  and  $\sigma$  for the FD channel for 206 periods calculated using the envelope calculations in TRACEWIN. The stop band calculated by the eigenvalue analysis is also shown in the figure. We see that

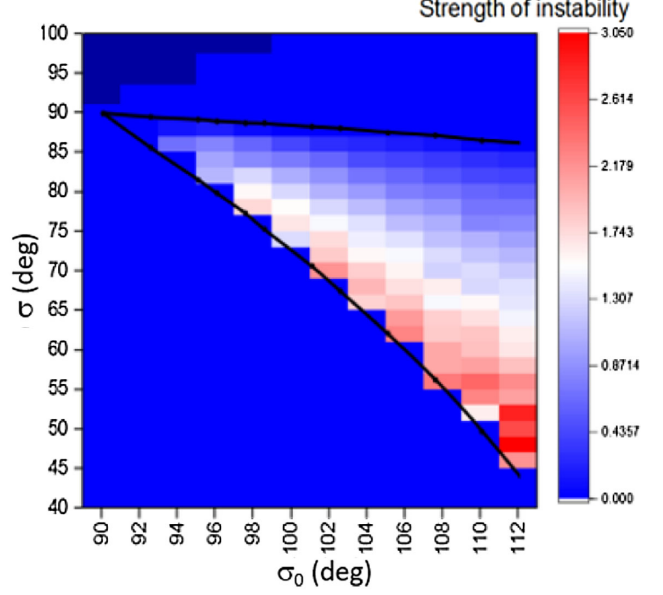


FIG. 5. The contour plot shows the strength of the envelope instability ( $\Delta a/a$ ) for different values of  $\sigma_0$  and  $\sigma$  for the FD channel in Fig. 1, for 206 periods. The width of the stopband from envelope calculations is also shown.

the width of the stop band calculated agrees quite well with that calculated by the eigenvalue analysis.

It can be seen from Fig. 5 that in the envelope instability stop band, for each value of  $\sigma_0$ , the strength of the instability increases as  $\sigma$  decreases (i.e., as the beam current increases). The strength of the instability is maximum at the lower end of the stop band. Also, as  $\sigma_0$  increases, the maximum value of the strength in the stop band increases.

### III. SINGLE PARTICLE RESONANCES

Single particle resonances are incoherent effects. The resonance condition is

$$mk_{xy} = 360^\circ$$

where  $k_{xy}$  is the single particle transverse phase advance per period. Here  $m$  is the resonance order [45]. In general, the  $m$ th-order resonance will be excited only when

$$\sigma_0 \geq 360^\circ/m$$

The fourth-order particle resonance was first predicted in 2009 [16] and subsequently seen experimentally at UNILAC, GSI [26]. It is characterized by the formation of a fourfold structure in phase space, and particles lying within the fourfold structure have a tune of 0.25 where the tune is defined as  $k_{xy}/2\pi$ .

The envelope calculations using the KV envelope equation or matrix multiplication, as discussed above, will give

only the collective response of the beam as a whole but no information about the single particle effects. These can be studied using the particle-core model, where the space charge calculated from the initial beam envelope is kept fixed and the macroparticles are tracked as a response to this force.

The equations of motion of a single particle with space charge are written as

$$\frac{d^2s}{ds^2} - k_x(s)x(s) - KF_{sc,x}(s) = 0, \quad (3)$$

$$\frac{d^2y}{ds^2} - k_y(s)y(s) - KF_{sc,y}(s) = 0, \quad (4)$$

where,

$$F_{sc,x}(s) = \frac{x(s)}{X(s)[X(s) + Y(s)]}, \quad |x(s)| \leq X(s)$$

$$F_{sc,x}(s) = \frac{x(s)}{x(s)^2 + |x(s)|\sqrt{x(s)^2 + Y(s)^2 - X(s)^2}}, \quad |x(s)| > X(s).$$

Similarly,

$$F_{sc,y}(s) = \frac{y(s)}{Y(s)[X(s) + Y(s)]}, \quad |y(s)| \leq Y(s),$$

$$F_{sc,y}(s) = \frac{y(s)}{y(s)^2 + |y(s)|\sqrt{y(s)^2 + X(s)^2 - Y(s)^2}}, \quad |y(s)| > Y(s).$$

These expressions are valid for uniform density beams [42,45,46] with  $\frac{x^2}{X^2} + \frac{y^2}{Y^2} = 1$ . Equations (3) and (4) are not coupled in  $x(s)$  and  $y(s)$  (for the current study) and therefore we can independently analyze these single particle equations. Simulations using the particle-core model have been done for 1000 test particles lying between 0 and 3 times the rms envelope for different values of  $\sigma$ .

The envelope is calculated using envelope Eqs. (1) and (2) and the single particle dynamics is studied for this envelope. In this model, the self-consistent interactions among the particles are not considered, i.e., the contribution of the self-fields of the individual particles is not considered. The particle-core model will thus give only the single particle behavior and allow us to separate the single particle behavior from the collective behavior.

For  $\sigma_0 = 100^\circ$ , we can see from Fig. 2 that the stop band for the envelope instability lies in the region  $72.8^\circ < \sigma < 88.2^\circ$ . Simulations using the particle-core model have been done for  $\sigma$  lying within and outside the envelope instability stop band and the Poincare plots of the individual particles are shown in Fig. 6. The tunes of the test

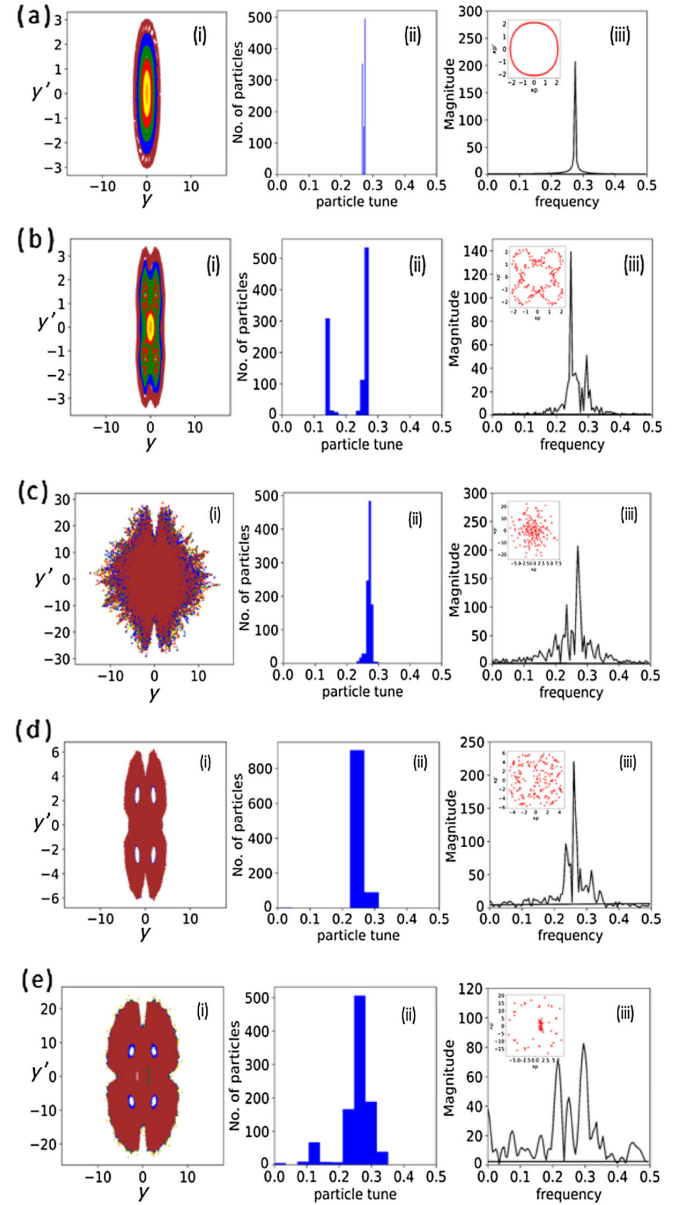


FIG. 6. Poincare plot in  $y'$ - $y$  phase space, particle FFT histograms of 1000 test particles using the particle-core model and the FFT of a test particle along with the phase space of the test particle in the inset, for (a)  $\sigma_0 = 100^\circ$ ,  $\sigma = 99^\circ$ , (b)  $\sigma_0 = 100^\circ$ ,  $\sigma = 89.8^\circ$  (above the instability region), (c)  $\sigma_0 = 100^\circ$ ,  $\sigma = 75.9^\circ$  (inside the instability region; here the effect of variation of the beam envelope due to the envelope instability is also included), (d)  $\sigma_0 = 100^\circ$ ,  $\sigma = 65.7^\circ$  (below the instability region), and (e)  $\sigma_0 = 100^\circ$ ,  $\sigma = 28^\circ$  (below the instability region). The test particles are distributed at the entry of the channel to lie between 0 and 3 times the rms beam size.

particles are calculated by doing a fast Fourier transform (FFT) for all the particle trajectories. The maximum amplitude frequency peak of the FFT is considered and plotted in the form of histograms in Fig. 6.

Figure 6(a) is for an initial condition lying far above the envelope instability stop band ( $\sigma_0 = 100^\circ$ ,  $\sigma = 99^\circ$ ). The beam current is small and space charge forces are not very high. The FFT analysis shows a very sharp tune corresponding to a beam phase advance of  $99^\circ$  as seen in Fig 6(a) (ii). The absence of any other tune value in the FFT suggests that no other single particle resonances are excited. For  $< 90^\circ$ , it can be seen from Figs. 6(b) to 6(e), lying outside the instability stop band, in the regions above and below the envelope instability, a fourfold structure is formed in the Poincare plot. Figure 6(b) is for a case  $< 90^\circ$  lying above the instability stop band. The fourth-order resonance gets excited for this condition and tunes close to 0.25 are observed in the FFT histogram as seen in Fig. 6(b)(ii). The full FFT of a test particle lying in the fourth-order resonance (tune = 0.249) is shown in Fig. 6(b)(iii) with the phase space of the particle shown in the inset. The FFT histogram of the particle trajectories shows tunes of particles close to 0.25 which suggests the excitation of the fourth-order single particle resonance when  $\sigma_0 > 90^\circ$  and for particles satisfying the fourth-order resonance condition,  $mk_{xy} = 360^\circ$ . In Fig. 6(c),  $\sigma_0 = 100^\circ$ ,  $\sigma = 75.9^\circ$  lies inside the instability region. Here, due to the envelope instability, a stable fixed point does not exist for the matched beam [Fig 4(b)]. Using the unstable beam envelope and studying the behavior of the test particles, we find that the single particle fourth-order resonance has been suppressed in this region. The particle-core model shows that fourth-order resonance is excited in the initial few lattice periods and gets suppressed once the beam envelope becomes unstable. FFT of the test particle in Fig. 6(c)(iii) shows evidence of more than one frequency having a comparable magnitude in the instability stop band region. As the beam current increases and the tune depression decreases, we see a large spread in the tune values in the FFT plot as seen in Figs. 6(d) and 6(e). This is in addition to the tunes of particles around 0.25. This suggests the formation of higher-order single particle resonances in the beam, in addition to the fourth-order resonance. We also see that the excursion in the Poincare phase space plots increases as the tune depression decreases.

For small beam currents, the analysis gives a general linear shift in the particle tunes. However, at higher currents, or lower depressed tunes, strong nonlinearity results in the appearance of additional resonances at different tunes. This may result in chaotic motion of the particles, resulting from resonance overlap, as seen in the broadening of the particle tunes in Fig. 6(e)(ii). The FFT of a test particle no longer shows a single dominant peak but shows multiple peaks, as can be seen in Fig 6(e)(iii). The beam remains matched in this case.

In this model, the transverse beam emittances of the beam envelope,  $\epsilon_x$  and  $\epsilon_y$ , are assumed to be constant as the envelope does not evolve self-consistently in these calculations. To study the contribution of the single particle effects, we define the single particle emittance  $E_x$  and  $E_y$  of the particles as [46]

$$E_x = \sqrt{\left(\frac{x}{X}\right)^2 + \left(\frac{X'x - x'X}{\epsilon_x}\right)^2}$$

and

$$E_y = \sqrt{\left(\frac{y}{Y}\right)^2 + \left(\frac{Y'y - y'Y}{\epsilon_y}\right)^2}.$$

The single particle emittances are calculated in scaled coordinates— $x/X$  and  $(X'x - x'X)/\epsilon_x$  for  $x$ , and  $y/Y$  &  $(Y'y - y'Y)/\epsilon_y$  for  $y$ —and are different from the beam emittance. The single particle emittance in scaled units gives a better idea of the excursion of the particle from the center, relative to the matched beam core. For a stable beam, when the single particle emittance is unity, the particle is at the beam envelope. As the particle goes further out from the center, the value of the single particle emittance increases. Average emittance is then defined by taking the average of the single particle emittance for the 1000 test particles and average emittance growth is observed as tune depression is varied.

The variation of the average emittance growth as a function of the tune depression ( $\eta = \sigma/\sigma_0$ ) for  $\sigma_0 = 100^\circ$  is shown in Fig. 7.

We see that the average emittance increases in the stopband of the envelope instability. Qualitatively, the emittance increase in the stopband also agrees well with the strength of the envelope instability calculated from the change in beam envelope in Fig. 5. We also see an increase in emittance at lower values of tune depression. The envelope calculations do not show any collective effects that lead to beam degradation below and above the instability stop band. Hence the emittance increase at lower tune depression values is only due to the single particle resonances. At lower values of the tune depression, we see from Fig. 6(a), a spread in the values of particle tunes. As the tune depression decreases, the conditions for several single particle resonances are satisfied and all these

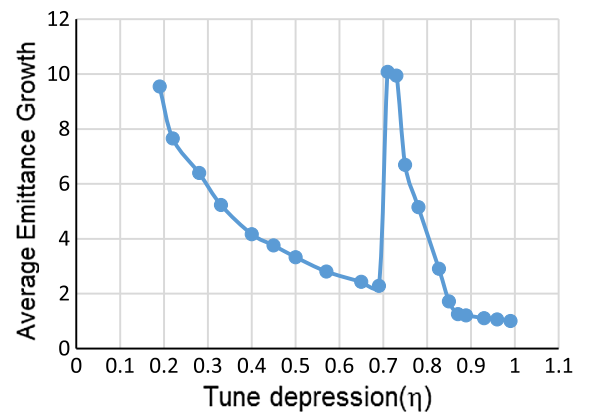


FIG. 7. Average transverse emittance growth for 1000 test particles as a function of tune depression for  $\sigma_0 = 100^\circ$ , calculated from the particle-core model.

resonances are excited which could lead to an increase in the beam emittance.

#### IV. SELF-CONSISTENT PIC SIMULATIONS

The particle-core model discussed above does not include the self-consistent feedback and gives an idea only about the incoherent behavior of the particles. The self-consistent PIC simulations include both, the coherent and incoherent response of the beam. We performed self-consistent PIC simulations to see the complete behavior of the beam that includes both the coherent and incoherent beam dynamics. The TRACEWIN code was used for these studies.

Figure 8 shows the variation of transverse emittance growth of the beam ( $\varepsilon_f/\varepsilon_i$ ) with the tune depression  $\sigma/\sigma_0$  of the beam for  $\sigma_0 = 100^\circ$  for a Gaussian beam through the FD channel shown in Fig. 1 for 206 periods. Here  $\varepsilon_f$  is the final transverse emittance of the beam and  $\varepsilon_i$  is the initial transverse emittance of the beam. The extent of the envelope instability stop band from envelope calculations for  $\sigma_0 = 100^\circ$  ( $72.8^\circ < \sigma < 88.2^\circ$ ) is indicated in black.

If we compare Fig. 7 with Fig. 8, we see that the pattern of emittance increase is similar between the particle-core model and PIC simulations except in the region of the envelope instability. We see that the width of the region of emittance increase under the envelope instability region is now wider than that indicated by envelope calculations and the particle-core model. From PIC simulations, we see that the peak of emittance increase extends beyond the region of envelope instability calculated by the envelope equations at the lower threshold limit of the envelope instability stop band. For lower tune depression values, the emittance increase pattern agrees quite well. The beam envelope

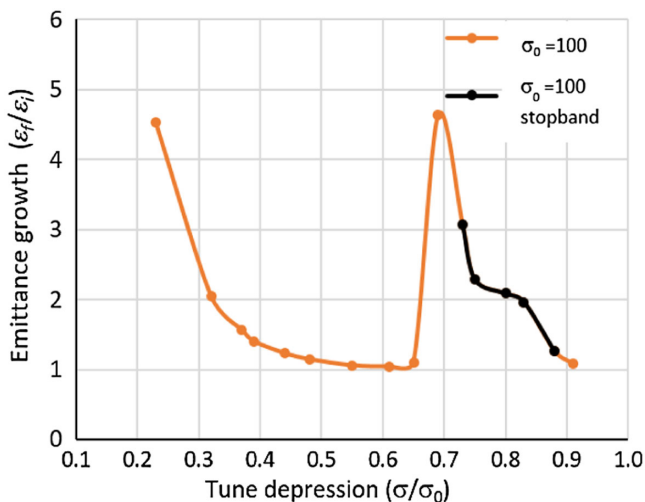


FIG. 8. Variation of transverse emittance growth of the beam ( $\varepsilon_f/\varepsilon_i$ ) with the tune depression  $\sigma/\sigma_0$  of the beam for  $\sigma_0 = 100^\circ$ . Also shown is the envelope instability stop band for  $\sigma_0 = 100^\circ$ , calculated from the KV envelope equations.

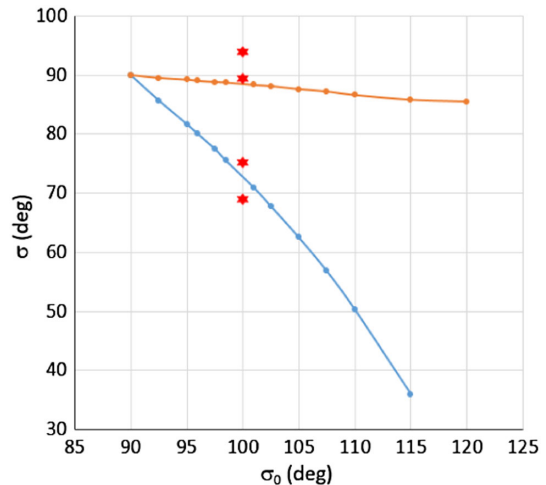


FIG. 9. Location of the points (initial condition) with respect to the stop band for which analysis is done for the FD lattice.

remains stable in the envelope calculations, suggesting that the emittance increase in the region below the envelope instability is mainly due to the incoherent single particle effects. The possibility of higher-order coherent modes of the beam envelope is also ruled out as these are Landau damped in a Gaussian beam [47].

To understand the processes responsible for the increase in beam emittance, we analyzed the evolution of the beam in the different regions mentioned below for an initially well-matched  $3\sigma$  Gaussian beam with  $\sigma_0 = 100^\circ$  through the FD lattice shown in Fig. 1.

- (1) Initial  $\sigma$  greater than  $90^\circ$  ( $\sigma = 94^\circ$ ).
- (2) Initial  $\sigma$  lying above the envelope instability stop band and less than  $90^\circ$  ( $\sigma = 89^\circ$ ).
- (3) Initial  $\sigma$  lying in the envelope instability stop band ( $\sigma = 75^\circ$ ).
- (4) Initial  $\sigma$  lying below the envelope instability stop band ( $\sigma = 69^\circ$ ).

These points are plotted with respect to the stop band in Fig. 9. All the calculations have been done using 100,000 macroparticles in TRACEWIN.

##### 1. Initial $\sigma$ greater than $90^\circ$

The results of the PIC simulation of a well-matched Gaussian beam through the FD channel for  $\sigma_0 = 100^\circ$  and initial  $\sigma = 94^\circ$  are shown in Fig. 10. The beam is stable and no increase in emittance is seen. The beam phase space in  $x$  and  $y$  at 3 m from the entry of the channel and at the end of 206 periods is shown in Fig. 11. It can be seen that the beam is stable in phase space and no evidence of envelope instability or single particle resonance is seen.

##### 2. Initial $\sigma$ less than $90^\circ$ and lying above the envelope instability stop band

For an initially well-matched Gaussian beam with initial phase advance lying above the envelope instability region

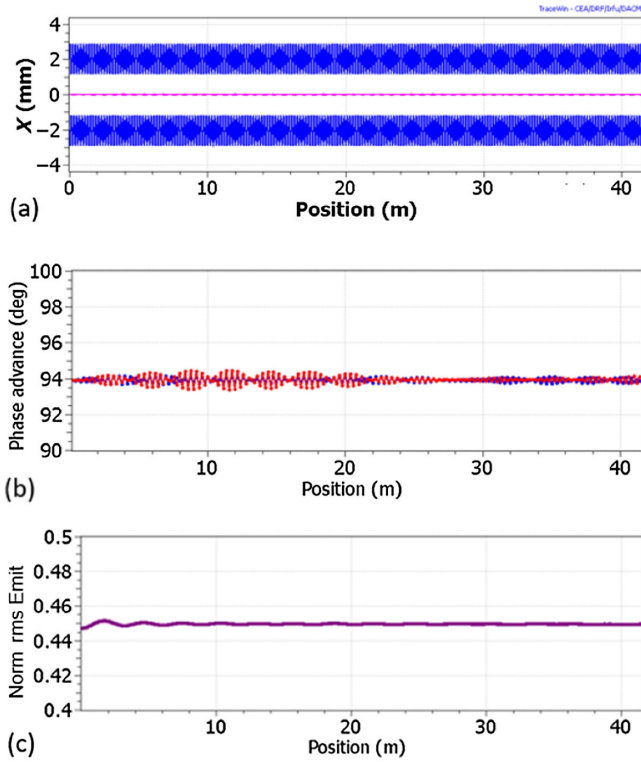


FIG. 10. (a) The beam envelope in  $x$  from PIC simulations, (b) beam phase advance, and (c) transverse emittance along the FD lattice, for  $\sigma_0 = 100^\circ$  and initial  $\sigma = 94^\circ$  for an initially well-matched Gaussian beam in the FD channel.

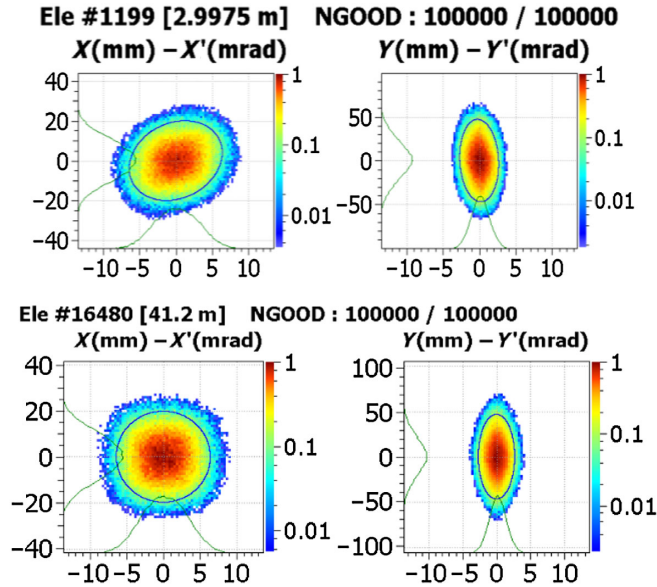


FIG. 11. Beam phase space at two different locations along the FD lattice for  $\sigma_0 = 100^\circ$  and initial  $\sigma = 94^\circ$ .

but less than  $90^\circ$  ( $\sigma_0 = 100^\circ$  and  $\sigma = 89^\circ$ ), the beam envelope in  $x$  from envelope calculations in TRACEWIN, beam envelope in  $x$  from PIC simulations in TRACEWIN, beam phase advance and transverse emittance are shown in

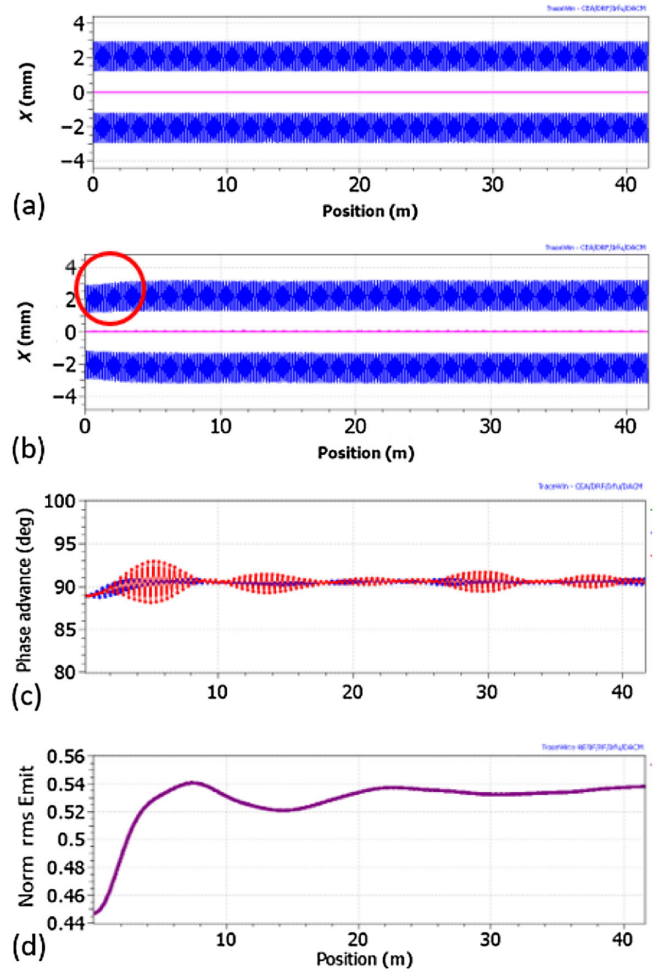


FIG. 12. (a) The beam envelope in  $x$  from envelope calculations, (b) the beam envelope from PIC simulations, (c) beam phase advance, and (d) transverse emittance along the FD lattice for  $\sigma_0 = 100^\circ$ , and initial  $\sigma = 89^\circ$  for an initially well-matched Gaussian beam in the FD channel.

Figs. 12(a)–12(d), respectively. The beam phase space in  $x$  and  $y$  at various locations along the lattice is shown in Fig. 13.

From Fig. 12(b), we see that the beam size increases initially and then becomes constant. This increase in beam size is not seen in the envelope calculations [Fig. 12(a)] and hence is due to single particle effects. Figure 13 shows the formation of a fourfold structure in beam phase space that gradually fades away after about 4 m. This suggests that the fourth-order particle resonance is excited initially. The beam emittance also increases in this region [Fig. 12(d)]. We see that, as the beam evolves self-consistently, the beam phase advance also increases, and once the beam phase advance is greater than  $90^\circ$ , the beam stabilizes at a new equilibrium value. Here the fourth-order resonance also fades away. As the beam phase advance always remains outside the envelope instability stop band, the envelope instability is not excited.

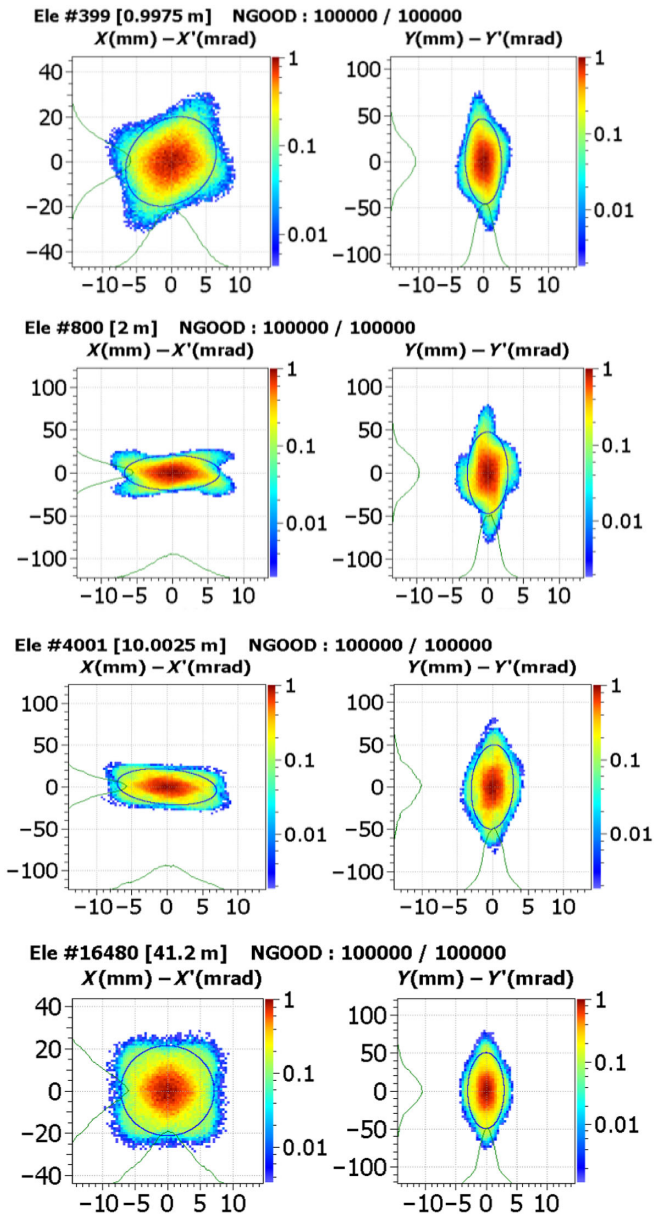


FIG. 13. Beam phase space at various locations along the FD lattice for  $\sigma_0 = 100^\circ$  and initial  $\sigma = 89^\circ$ .

### 3. Initial $\sigma$ lying inside the envelope instability stop band

Figures 14 and 15 show the results for an initially well-matched Gaussian beam with initial phase advance lying inside the envelope instability region. The depressed phase advance here is  $75^\circ$  which lies within the envelope instability stop band.

From Figs. 14(a) and 14(b), we see that instability in the beam envelope is seen both in the envelope calculations as well as the PIC calculations. From Fig. 14(d), we see that initially, up to a distance of about 4 m, the emittance increases gradually. It can be seen from Fig. 15 that the beam distribution of the initially well-matched Gaussian beam in phase space evolves into a fourfold structure in a

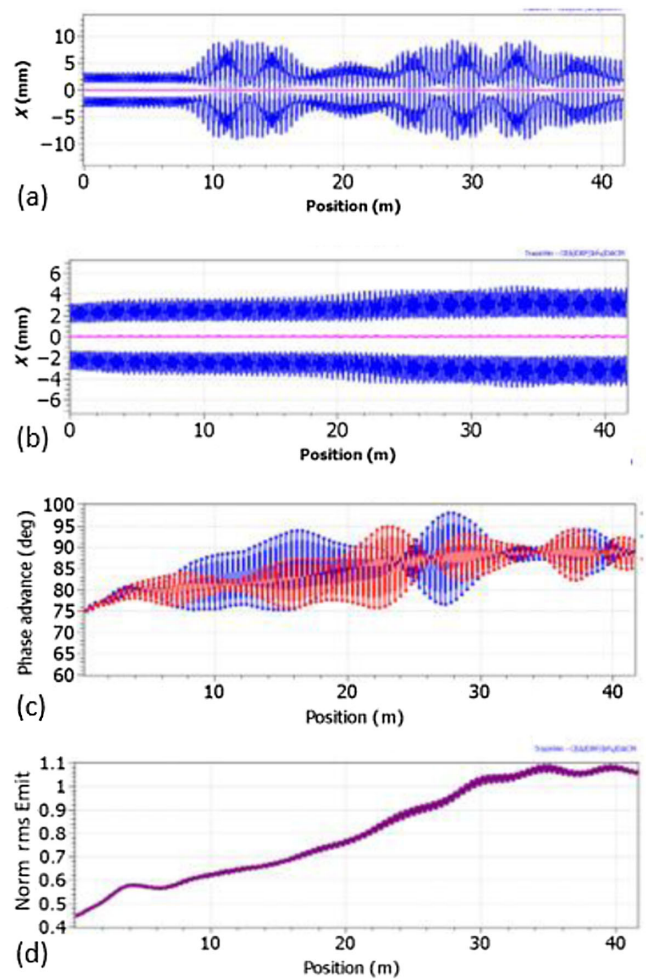


FIG. 14. (a) The beam envelope in  $x$  from envelope calculations, (b) the beam envelope from PIC simulations, (c) beam phase advance, and (d) transverse emittance along the FD lattice for  $\sigma_0 = 100^\circ$ , and initial  $\sigma = 75^\circ$  for an initially well-matched Gaussian beam in the FD channel.

couple of lattice periods. At around 4 m, the fourfold structure in beam phase space also starts evolving into a twofold structure. The rms emittance increases and we see disturbances in the beam envelope oscillations following which, at about 32 m, both the rms emittance and the beam envelope stabilize at higher values. The beam phase advance also keeps on increasing and the stabilization of the beam to a new equilibrium value happens when the phase advance settles to a value slightly above  $90^\circ$ . In this region, the conditions for neither the envelope instability nor the fourth-order single particle resonance are satisfied.

These studies show and reconfirm the findings of [48] that in an initially well-matched beam, the fourth-order particle resonance is excited first and the envelope instability is excited subsequently. Once the envelope instability is excited, it dominates over the fourth-order particle resonance. This is evident from the beam phase space evolving from the fourfold structure into the twofold

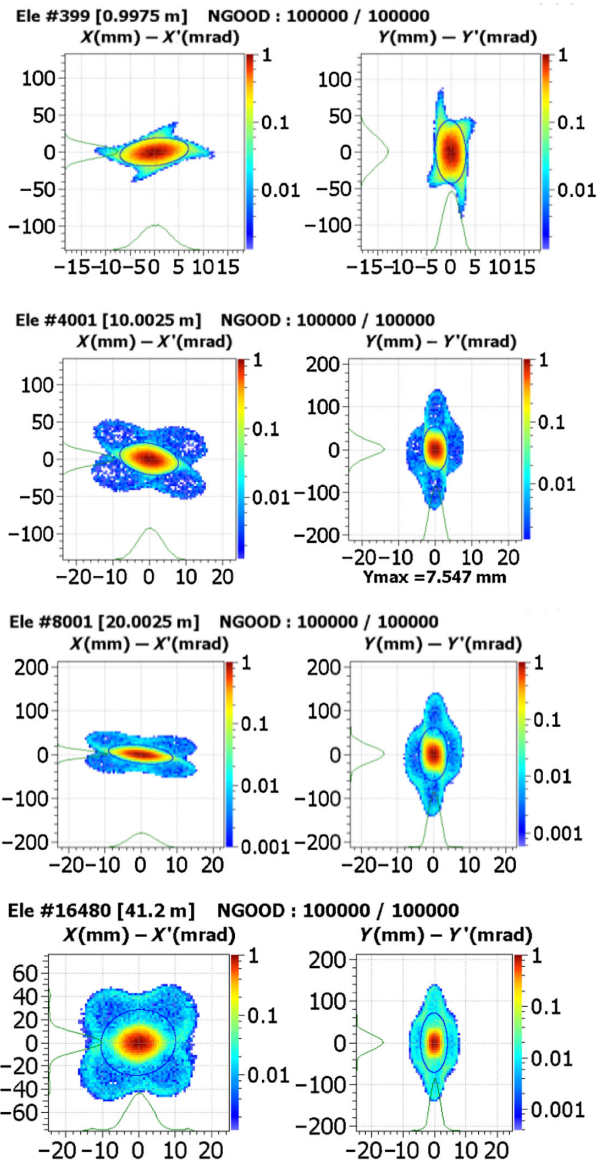


FIG. 15. Beam phase space at various locations along the FD lattice for  $\sigma_0 = 100^\circ$  and initial  $\sigma = 75^\circ$ .

structure. Within the envelope instability stop band, the initial mismatch plays a very important role in determining which phenomenon is excited first. For an initially well-matched beam in the channel, the fourth-order particle resonance is excited first and the envelope instability gets excited later. In the presence of an initial mismatch of 0.1 in  $x$  and  $y$ , the envelope instability is excited immediately and dominates over the fourth-order particle resonance. This can be seen in Fig. 16. We see that the beam envelope varies erratically at the entrance of the channel for the mismatched beam while for the matched beam, the beam envelope first increases gradually due to the fourth-order resonance and then after some time, erratic variations in the envelope are seen. Figure 17 shows the beam phase space at a distance of about 4 m from the entry of the channel for initially

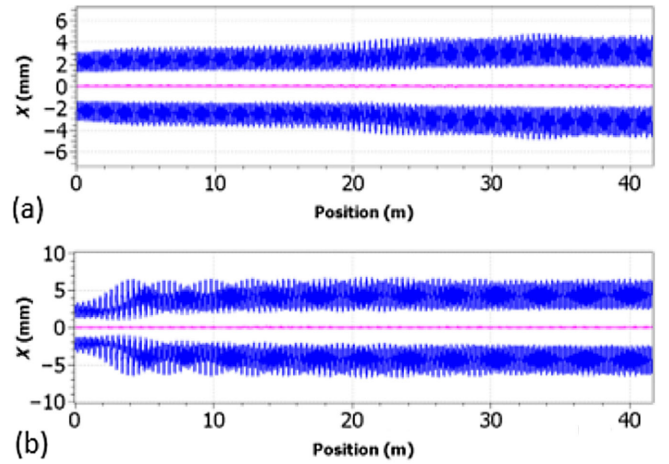


FIG. 16. Beam envelope from PIC simulations in  $x$  for  $\sigma_0 = 100^\circ$  and  $\sigma = 75^\circ$  for (a) initially matched beam, and (b) initial mismatch of 0.1 in  $x$  and  $y$  for 206 FD periods.

matched and mismatched beams. It can be seen that for the well-matched beam, the fourth-order particle resonance is excited, while, in the presence of an initial mismatch, the envelope instability is excited immediately and dominates over the fourth-order resonance. Thus, the initial mismatch decides how soon the envelope instability is excited.

Here the mismatch factor in  $x$  ( $M_x$ ) between the two ellipses  $\varepsilon = \gamma x^2 + 2\alpha x x' + \beta (x')^2$  (matched ellipse) and  $\varepsilon = Gx^2 + 2Ax x' + B(x')^2$  (mismatched ellipse) is defined as [37]

$$M_x = \sqrt{\left[ \frac{1}{2} (R + \sqrt{R^2 - 4}) \right]} - 1,$$

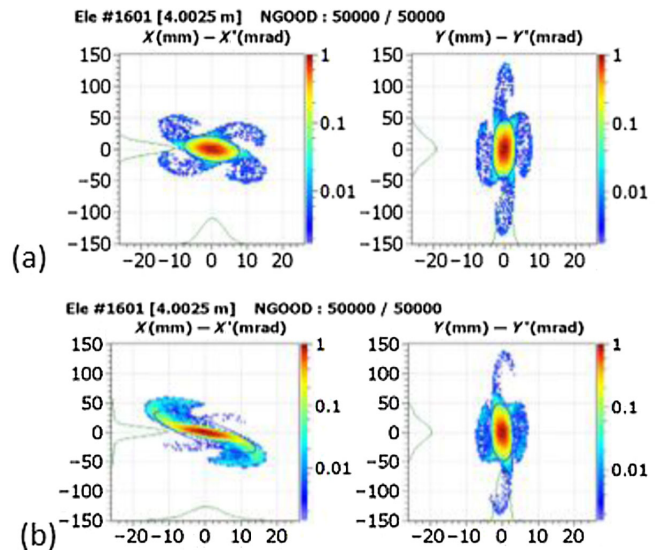


FIG. 17. Beam phase space at about 3.5 m from the entrance of the FD channel for (a) initially matched beam and (b) initial mismatch of 0.1 in  $x$  and  $y$ .

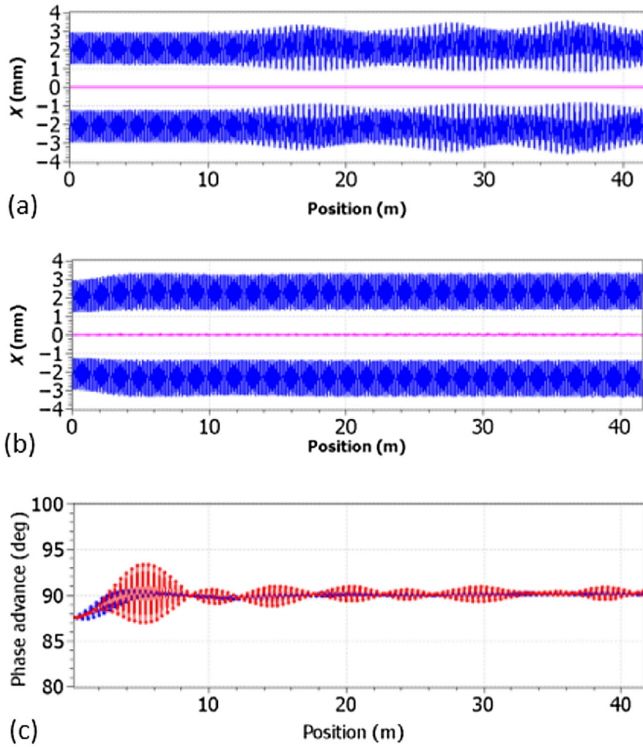


FIG. 18. (a) The beam envelope in  $x$  from envelope calculations, (b) the beam envelope from PIC simulations, and (c) beam phase advance for  $\sigma_0 = 100^\circ$  and  $\sigma = 88^\circ$ .

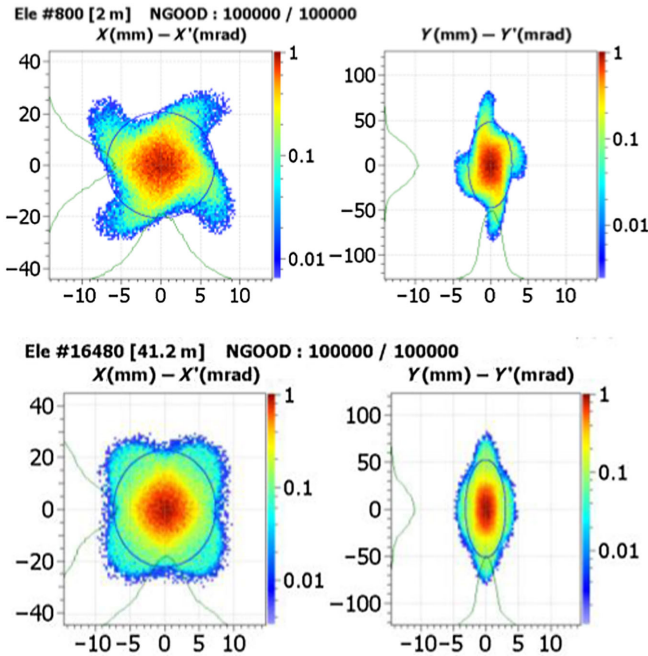


FIG. 19. Beam phase space at 2 and 41.2 m along the FD lattice for  $\sigma_0 = 100^\circ$  and initial  $\sigma = 88^\circ$ .

where  $R = \beta G + B\gamma - 2\alpha A$ ,  $\alpha$ ,  $\beta$ , and  $\gamma$  are the Twiss parameters of the matched beam and  $A$ ,  $B$ , and  $G$  are the Twiss parameters of the mismatched beam in the phase space  $xx'$ . The mismatch in  $y$  and  $z$  is similarly defined.

For well-matched beams with beam phase advance lying within the envelope instability stop band very close to the upper end of the stop band, the PIC calculations show that the envelope instability is not excited and only the fourth-order resonance is excited. This can be seen for  $\sigma_0 = 100^\circ$ ,  $\sigma = 88^\circ$ , which lies within the envelope instability stop band. This happens because initially when the fourth-order resonance is excited, the beam phase advance increases and the beam comes out of the instability region before the instability can be excited. This can be seen in Fig. 18. The envelope instability is clearly seen from the envelope calculations where the beam envelope varies erratically [Fig. 18(a)]. On the other hand, the beam envelope from

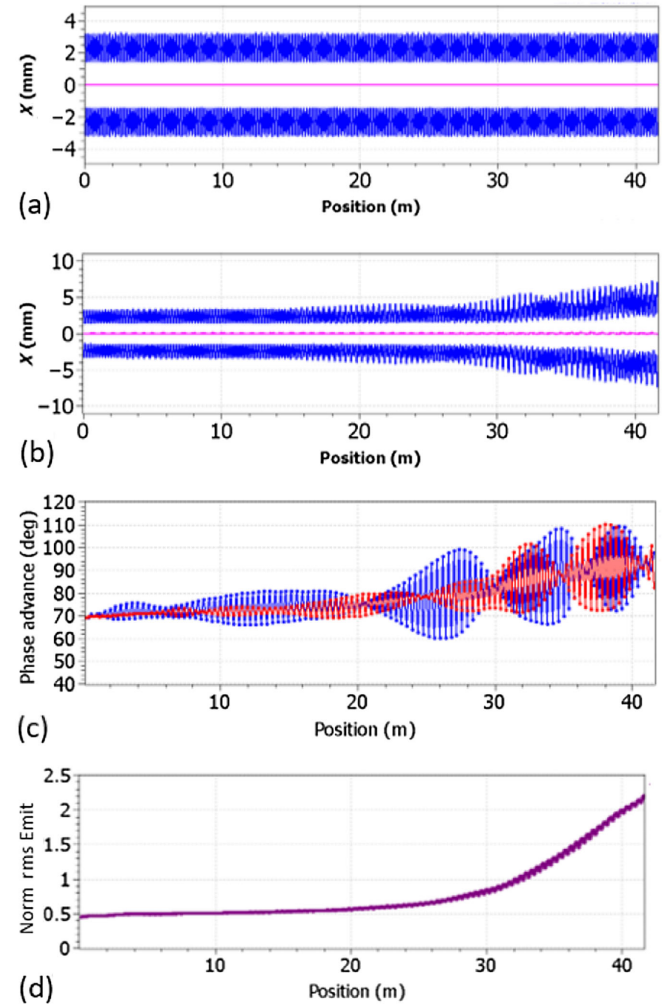


FIG. 20. (a) The beam envelope in  $x$  from envelope calculations, (b) the beam envelope from PIC simulations, (c) beam phase advance, and (d) transverse emittance along the FD lattice for  $\sigma_0 = 100^\circ$ , and initial  $\sigma = 69^\circ$  for an initially well-matched Gaussian beam in the FD channel.

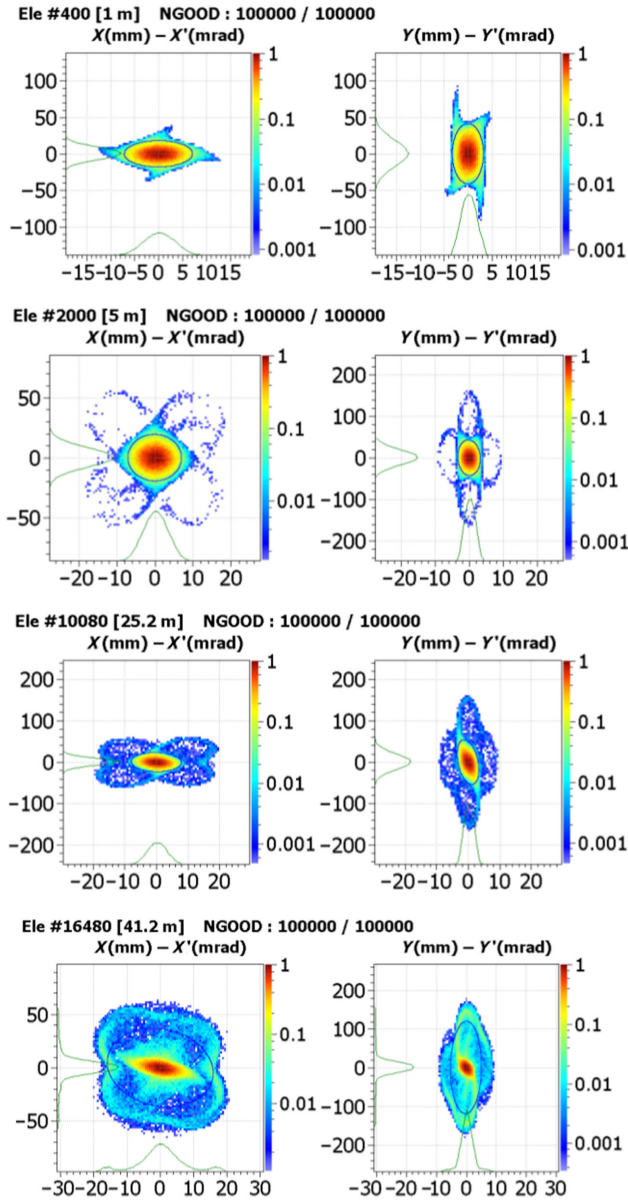


FIG. 21. Beam phase space at various locations along the FD lattice for  $\sigma_0 = 100^\circ$  and initial  $\sigma = 69^\circ$ .

PIC calculations [Fig. 18(b)] shows a gradual increase in beam size which stabilizes after some time as the beam phase advance crosses  $90^\circ$ . The beam phase space in Fig. 19 also shows evidence of the fourth-order particle resonance but no envelope instability.

#### 4. Initial $\sigma$ lying below the envelope instability stop band

The results of the PIC calculations for an initially well-matched beam with depressed beam phase advance  $\sigma = 69^\circ$ , lying below the lower bound of the envelope instability stop band ( $\sigma = 72.2^\circ$ ), are shown in Figs. 20 and 21. From the beam phase space, we can see that initially, the fourth-order particle resonance is excited. We see from Fig. 20(c) that as the beam evolves, the beam phase

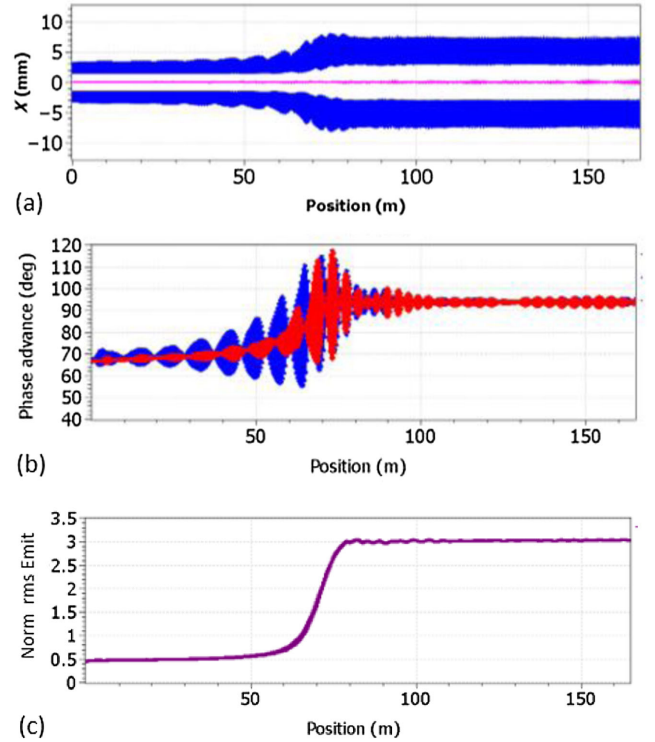


FIG. 22. (a) The beam envelope in  $x$  from PIC simulations, (b) beam phase advance, and (c) transverse emittance along the FD lattice for  $\sigma_0 = 100^\circ$  and initial  $\sigma = 67^\circ$  for an initially well-matched Gaussian beam, for 824 FD periods.

advance increases and the beam enters into the envelope instability region ( $\sigma > 72.8^\circ$ ). Here, the envelope instability gets excited. The beam emittance and phase advance increase and finally stabilize when the phase advance is just above  $90^\circ$ . This explains the peak in emittance growth for  $\sigma = 69^\circ$  in Fig. 8, which lies just below the envelope instability region. The beam evolves self-consistently due to the fourth-order resonance that results in the gradual increase of the beam phase advance. Once the phase advance enters the envelope instability region, the envelope instability gets excited.

For  $\sigma = 67^\circ$ , the increase in phase advance due to the fourth-order resonance is not sufficient to push the beam into the envelope instability region in 206 periods (41.2 m). However, if we simulate a longer channel of 824 periods (164.8 m), we see that the phase advance increases gradually and the beam will eventually enter the instability region. Once the envelope instability is excited, the beam phase advance and emittance increase rapidly and the beam stabilizes after the phase advance is just greater than  $90^\circ$ . This can be seen in Fig. 22.

Figure 23 shows the variation of transverse emittance growth  $\epsilon_f/\epsilon_i$  of the beam with the tune depression  $\eta$  for  $\sigma_0 = 100^\circ$  for 206 and 824 FD periods. For 206 periods, we see a peak for  $\sigma = 69^\circ$  while for 824 periods, we see a peak for  $\sigma = 65^\circ$ . For a larger number of periods,  $\sigma = 65^\circ$  is

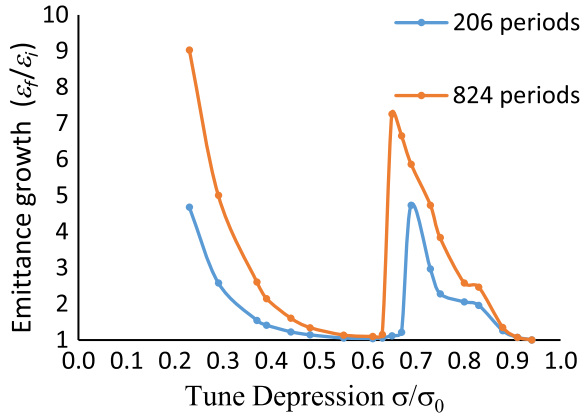


FIG. 23. Variation of transverse emittance growth of the beam  $\epsilon_f/\epsilon_i$  with the tune depression  $\sigma_0/\sigma$  of the beam for  $\sigma_0 = 100^\circ$ , for 206 and 824 FD periods.

pushed into the instability region. From Fig. 22, we can see that, for 206 periods (41.2 m), the fourth-order resonance is seen and the beam phase advance has still not entered the instability region. If, however, we increase the number of periods, we can see that envelope instability gets excited after around 50 m, and the beam emittance and phase advance increase until the beam exits the instability region

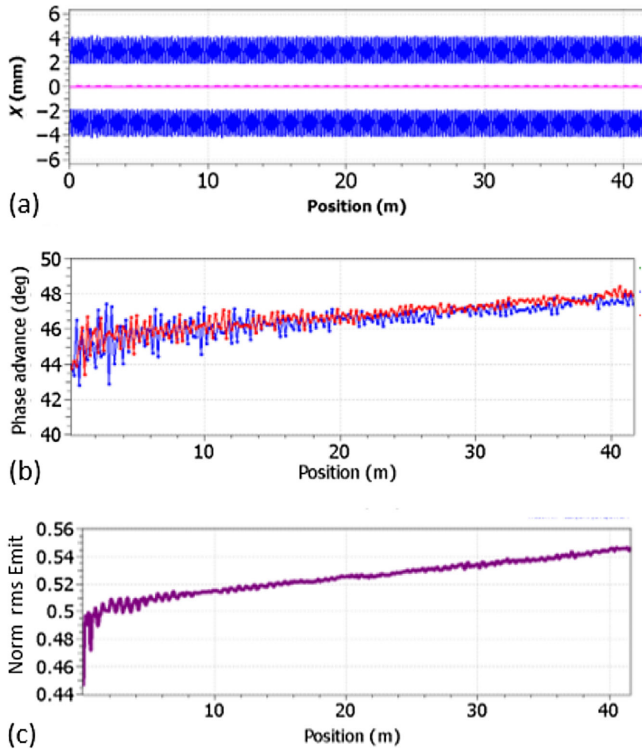


FIG. 24. (a) The beam envelope in  $x$  from PIC simulations, (b) beam phase advance, and (c) transverse emittance along the FD lattice for  $\sigma_0 = 100^\circ$  and initial  $\sigma = 44^\circ$  for an initially well-matched Gaussian beam in the FD channel.

at around 80 m. Hence, the width of the emittance increase in the instability region is more for a longer channel.

For tune depression less than 0.45, we see, from Fig. 23, an increase in the beam emittance. In this region, the conditions for several higher-order single particle resonances are satisfied and hence due to overlapping of several higher-order single particle resonances, the beam behavior becomes chaotic and the beam emittance increases. The results for beam phase advance  $\sigma = 44^\circ$  are shown in Figs. 24 and 25.

Simulations were performed with different values of  $\sigma_0$  to study the variation of emittance growth with the tune depression. The results for  $\sigma_0 = 96^\circ, 100^\circ$ , and  $110^\circ$  for 206

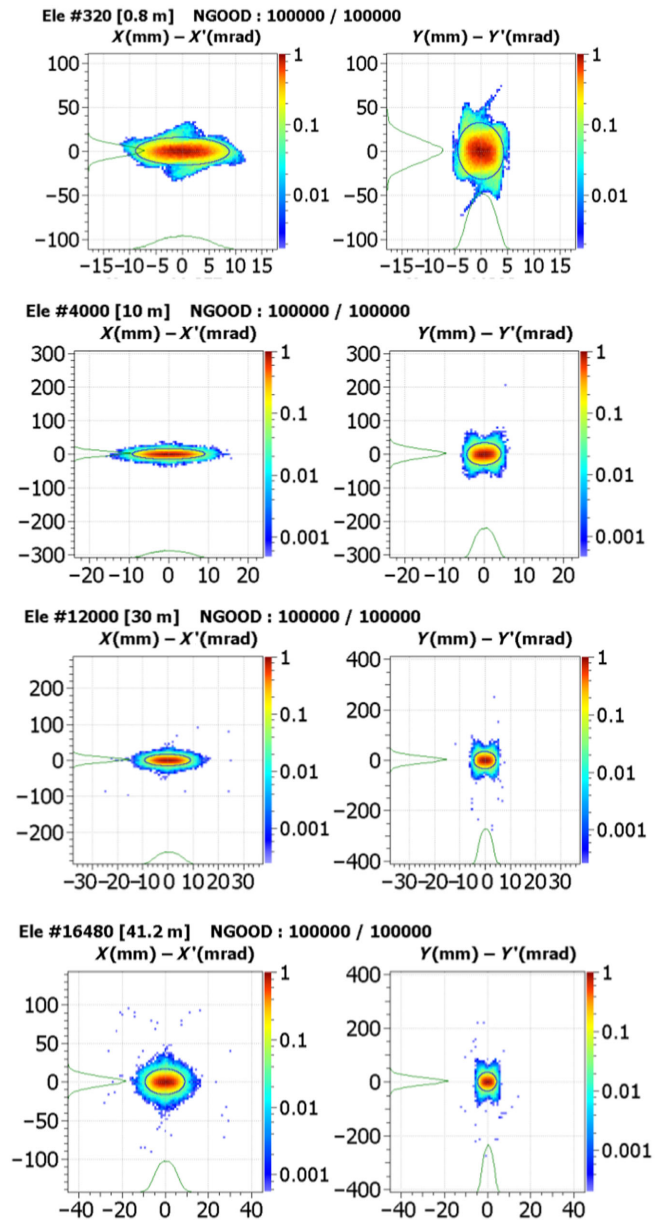


FIG. 25. Beam phase space at various locations along the FD lattice for  $\sigma_0 = 100^\circ$  and initial  $\sigma = 44^\circ$ .

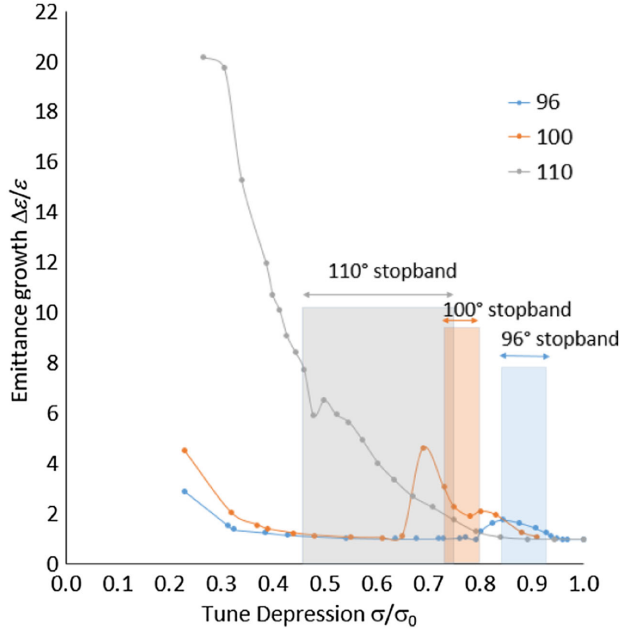


FIG. 26. Variation of transverse emittance growth of the beam  $\varepsilon_f/\varepsilon_i$  with the tune depression  $\sigma_0/\sigma$  of the beam for  $\sigma_0 = 90^\circ$ ,  $100^\circ$ , and  $110^\circ$ , for 206 FD periods. Also shown is the envelope instability stop band for  $\sigma_0 = 90^\circ$ ,  $100^\circ$ , and  $110^\circ$  calculated from the KV envelope equations.

FD periods are shown in Fig. 26. The envelope instability stop band is also marked in the figure for each value of  $\sigma_0$ . For all these cases, we see that the emittance increase extends beyond the envelope instability stop band. For  $\sigma_0 = 96^\circ$  and  $100^\circ$ , the emittance growth drops for tune depression values in the intermediate region and then begins to increase again for tune depression below 0.45. As discussed above, in this region, only the single particle effects are seen.

For  $\sigma_0 = 110^\circ$ , the emittance keeps on increasing continuously and there is no reduction in the emittance growth as the tune depression decreases. This is because the envelope instability stop band becomes wider as  $\sigma_0$  increases. The envelope instability stop band lies in the range  $50.3^\circ \leq \sigma \leq 86.6^\circ$ .

The emittance growth in the envelope instability region is consistent with the strength of the instability calculated in Fig. 5. For example, it can be seen that the emittance growth for  $\sigma_0 = 110^\circ$ ,  $\eta = 0.75$  is less than for  $\sigma_0 = 100^\circ$ ,  $\eta = 0.75$  as the strength of the instability is greater for the latter.

## V. CONCLUSIONS

We have carried out studies on a dc beam in an FD channel to distinguish between the coherent and incoherent effects for  $\sigma_0 > 90^\circ$ . In this region, the two main effects seen are the second-order envelope instability and the fourth-order particle resonance. The envelope instability

is a coherent effect in which the envelope as a whole becomes unstable. The stopband of the envelope instability lies over a range of  $\sigma$  values below  $\sigma = 90^\circ$  and can be calculated analytically using the KV envelope equations. The strength of the envelope instability has been calculated using the envelope calculations in TRACEWIN. It is seen that, qualitatively, the emittance increase in the instability region agrees very well with the calculated values of the strength of the envelope instability.

The incoherent effects, which are due to single particle dynamics, have been studied using the particle-core model. It is seen that the fourth-order particle resonance is excited in general for  $\sigma_0 > 90^\circ$  and  $\sigma < 90^\circ$  for the particles satisfying the resonance condition  $4k_{xy} = 360^\circ$ . This is confirmed by the formation of a fourfold structure in the Poincare plots and particle tunes around 0.25. It is seen that as tune depression decreases, single particle resonances other than the fourth-order resonances are also excited. This is confirmed by the appearance of tune spread in the FFT analysis for lower tune depression.

Self-consistent PIC simulations have been performed on the beam in the FD channel for  $\sigma_0 > 90^\circ$  to study the combined effect of the coherent and incoherent effects on the beam. The existence of fourth-order particle resonances is also confirmed by these studies. In PIC studies, as the beam evolves self-consistently in the channel, it is seen that in the instability region, for a well-matched beam, the fourth-order resonance is excited first and then the envelope instability is excited as the beam gets mismatched. If the beam is mismatched at the entry of the channel, the envelope instability is excited sooner and the fourth-order particle resonance is not seen. Once the envelope instability is excited, it dominates over the fourth-order resonance. We see that the fourfold structure evolves into a twofold or S-shape structure in phase space. PIC simulations show that when either of the effects is excited, as the beam evolves self-consistently, the beam emittance and beam phase advance increase. Even if the starting beam phase advance is below the instability region, if the phase advance increases and enters the instability stop band, the envelope instability is excited. Below the envelope instability stop band, the fourth-order resonance is excited and the beam can become unstable if the beam phase advance increases and enters the instability region. This can happen if the FD channel is long enough. The further the beam is from the lower bound of the envelope instability stop band, the longer the length of the channel is required to enter into the stop band. Hence the width of the large emittance growth stop band from the PIC simulation, using an initial Gaussian distribution, depends on the length of the channel. For  $\sigma_0 > 90^\circ$ , we see that the envelope instability is a more dangerous effect as it leads to a large increase in emittance and is excited for lower values of beam current and even for a shorter channel. The PIC simulations show that whether it is the envelope instability or single particle resonance, the

beam tries to come out of it. The beam phase advance increases and as it reaches the stable region where the instability and particle resonances cannot be excited, the beam stabilizes at a new equilibrium value. The beam size and emittances also stabilize at a new equilibrium value. With the help of the stop bands defined by the KV envelope equations and the self-consistent PIC simulations using TRACEWIN code, it is possible to differentiate between the single particle effects and the collective effects due to space charge in high intensity beams.

### ACKNOWLEDGMENTS

This work is supported by the Department of Atomic Energy, Government of India.

- 
- [1] P. Singh, S. Rao, R. Pande, T. Basak, S. Roy, M. Aslam, P. Jain, S. Srivastava, R. Kumar, P. Nema *et al.*, Accelerator development in India for ADS programme, *Pramana* **68**, 331 (2007).
- [2] J-L. Biarrotte, P. Pierini, D. Vandeplassche, A. Mueller, and H. Klein, Accelerator reference design for the MYRRHA European ADS demonstrator (2010), p. 79, <https://accelconf.web.cern.ch/LINAC2010/papers/tup020.pdf>.
- [3] T. Mukaiyama, Omega programme in Japan and ADS development at JAERI, in *Accelerator Driven Transmutation Technologies and Applications (Proc. 2nd Int. Conf., Prague, 1998)* (Citeseer, Prague, Czech Republic, 1999), pp. 1–5.
- [4] J. Tang, P. Cheng, H. Geng, Z. Guo, Z. Li, C. Meng, H. Ouyang, S. Pei, B. Sun, J. Sun *et al.*, Conceptual physics design for the China-ADS linac, in *Proceedings of the 25th Particle Accelerator Conference, PAC-2013, Pasadena, CA, 2013* (IEEE, New York, 2013), pp. 1397–1399, <https://accelconf.web.cern.ch/pac2013/papers/thpsm04.pdf>.
- [5] C. Park, H. Ahn, B. Choi, T. Eom, Y. Cho, J. Han, J. Lee, W. Park, S. Kang, W. Song *et al.*, The KOMAC project: Accelerator and transmutation project in Korea, in *KEK Proceedings* (National Laboratory for High Energy Physics, Tsukuba, Japan, 1998), pp. 319–322.
- [6] S. Henderson *et al.*, The Spallation Neutron Source accelerator system design, *Nucl. Instrum. Methods Phys. Res., Sect. A* **763**, 610 (2014).
- [7] S. N. Fu, S. X. Fang, and J. Wei, China spallation neutron source linac design, in *Proceedings of the 23rd International Linac Conference, LINAC-2006, Knoxville, TN, 2006* (JACoW, Knoxville, TN, 2006), pp. 165–167.
- [8] Jana Arup Ratan and Kumar Vinit, Beam optics studies and lattice design of the 1 GeV H- injector linac for ISNS, *Nucl. Instrum. Methods Phys. Res., Sect. A* **942**, 162299.
- [9] A. Pisent *et al.*, Design of the high current linac of SPES project, in *Proceedings of the 11th European Particle Accelerator Conference, Genoa, Italy, 2008* (EPSAG, Geneva, 2008), pp. 3545–3547.
- [10] PIP-II Conceptual Design Report, <https://lss.fnal.gov/archive/design/fermilab-design-2017-01.pdf> (2017).
- [11] J. Struckmeier and M. Reiser, Theoretical studies of envelope oscillations and instabilities of mismatched intense charged particle beams in periodic focusing channels, *Part. Accel.* **14**, 227 (1984), <https://s3.cern.ch/inspire-prod-files-e/e0fa3c604b003267fc56f8c0a829d2c0>.
- [12] Chao Li and Qing Qin, Space charge induced beam instability in periodic focusing channel, *Phys. Plasmas* **22**, 023108 (2015).
- [13] I. Hofmann, L. J. Laslett, L. Smith, and I. Haber, Stability of the Kapchinskij-Vladimirskij (K-V) distribution in long periodic transport systems, *Part. Accel.* **13**, 145 (1983), <https://cds.cern.ch/record/140869/files/p145.pdf>.
- [14] S.M. Lund and B. Bukh, Stability properties of the transverse envelope equations describing intense ion beam transport, *Phys. Rev. ST Accel. Beams* **7**, 024801 (2004).
- [15] J. Qiang, Three-dimensional envelope instability in periodic focusing channels, *Phys. Rev. Accel. Beams* **21**, 034201 (2018).
- [16] D. Jeon, L. Groening, and G. Franchetti, Fourth order resonance of a high intensity linear accelerator, *Phys. Rev. ST Accel. Beams* **12**, 054204 (2009).
- [17] D. Jeon and Kyung Ryun Hwang, Characteristics of the fourth order resonance in high intensity linear accelerators, *Phys. Plasmas* **24**, 063108 (2017).
- [18] S. Machida, Space-charge-induced resonances in a synchrotron, *Nucl. Instrum. Methods Phys. Res., Sect. A* **384**, 316 (1997).
- [19] Tomonori Uesugi, Shinji Machida, and Yoshiharu Mori, Experimental study of a half-integer resonance with space-charge effects in a synchrotron, *Phys. Rev. ST Accel. Beams* **5**, 044201 (2002).
- [20] S. Y. Lee and H. Okamoto, Space-charge dominated beams in synchrotrons, *Phys. Rev. Lett.* **80**, 5133 (1998).
- [21] A. V. Fedotov, I. Hofmann, R. L. Gluckstern, and H. Okamoto, Parametric collective resonances and space-charge limit in high-intensity rings, *Phys. Rev. ST Accel. Beams* **6**, 094201 (1998).
- [22] H. Okamoto *et al.*, Coherent and incoherent space-charge effects in high-intensity hadron rings, *J. Instrum.* **15**, P07017 (2020).
- [23] M. G. Tiefenback, Space-charge limits on the transport of ion beams in a long alternating gradient system, Ph.D. thesis, University of California, Berkeley, CA, 1986.
- [24] M. G. Tiefenback and D. Keefe, Measurements of stability limits for a space-charge-dominated ion beam in a long A.G. transport channel, *IEEE Trans. Nucl. Sci.* **NS-32**, 2483 (1985), [https://accelconf.web.cern.ch/p85/PDF/PAC1985\\_2483.PDF](https://accelconf.web.cern.ch/p85/PDF/PAC1985_2483.PDF).
- [25] L. Groening, W. Barth, W. Bayer, G. Clemente, L. Dahl, P. Forck, P. Gerhard, I. Hofmann, G. Riehl, S. Yarymyshev, D. Jeon, and D. Uriot, Benchmarking of measurement and simulation of transverse rms-emittance growth, *Phys. Rev. ST Accel. Beams* **11**, 094201 (2008).
- [26] L. Groening, W. Barth, W. Bayer, G. Clemente, L. Dahl, P. Forck, P. Gerhard, I. Hofmann, M. S. Kaiser, M. Maier, S. Mickat, T. Milosic, D. Jeon, and D. Uriot, Experimental evidence of the 90° stop band in the GSI UNILAC, *Phys. Rev. Lett.* **102**, 234801

- [27] Dong-O. Jeon, Experimental evidence of space charge driven resonances in high intensity linear accelerators, *Phys. Rev. Accel. Beams* **19**, 010101 (2016).
- [28] L. K. Martin, S. Machida, D. J. Kelliher, and S. L. Sheehy, A study of coherent, and incoherent resonances in high intensity beams using a linear Paul trap, *New J. Phys.* **21**, 053023 (2019).
- [29] I. Hofmann and O. Boine-Frankenheim, Space-charge structural instabilities and resonances in high-intensity beams, *Phys. Rev. Lett.* **115**, 204802 (2015).
- [30] Chao Li and Ya Liang Zhao, Envelope instability, and the fourth order resonance, *Phys. Rev. ST Accel. Beams* **17**, 124202 (2014).
- [31] D. Jeon, J. H. Jang, and H. Jin, Interplay of space-charge fourth order resonance and envelope instability, *Nucl. Instrum. Methods Phys. Res., Sect. A* **832**, 43 (2016).
- [32] Y. L. Cheon, S. H. Moon, M. Chung, and D. Jeon, Analysis on the stop band of fourth-order resonance in high-intensity linear accelerators, *Phys. Plasmas* **27**, 063105 (2020).
- [33] C. Chen and R. C. Davidson, Nonlinear resonances and chaotic behavior in a periodically focused intense charged-particle beam, *Phys. Rev. Lett.* **72**, 2195 (1994).
- [34] Chiping Chen and Ronald C. Davidson. Nonlinear properties of the Kapchinskij-Vladimirskij equilibrium, and envelope equation for an intense charged-particle beam in a periodic focusing field, *Phys. Rev. E* **49**, 5679 (1994).
- [35] I. M. Kapchinskij and V. V. Vladimirskij, Limitations of proton beam current in a strong focusing linear accelerator associated with the beam space charge, in *Proceedings of the International Conference on High Energy Accelerators, CERN, Geneva* (CERN, Geneva, Switzerland, 1959), p. 274
- [36] F. J. Sacherer (CERN), Rms envelope equations with space charge, *IEEE Trans. Nucl. Sci.* **18**, 1105 (1971).
- [37] TRACEWIN code, <http://irfu.cea.fr/dacm/logiciels/>.
- [38] A. J. Lichtenberg and M. A. Lieberman, *Regular and Stochastic Motion* (Springer, New York, NY, 1992).
- [39] T. P. Wangler, K. R. Crandall, R. Ryne, and T. S. Wang, Particle-core model for transverse dynamics of beam halo, *Phys. Rev. ST Accel. Beams* **1**, 084201 (1998).
- [40] Q. Qian, R. C. Davidson, and C. Chen, Chaotic particle motion and halo formation induced by charge non uniformities in an intense ion beam propagating through a periodic quadrupole focusing field, *Phys. Plasmas* **2**, 2674 (1995).
- [41] R. L. Gluckstern, Analytic model for halo formation in high current ion linacs, *Phys. Rev. Lett.* **73**, 1247 (1994).
- [42] T. S. F. Wang, Particle-core study of halo dynamics in periodic-focusing channels, *Phys. Rev. E* **61**, 855 (2000).
- [43] J. Qiang and R. D. Ryne, Beam halo studies using a three-dimensional particle-core model, *Phys. Rev. ST Accel. Beams* **3**, 064201 (2000).
- [44] Chao li, Zhicong Liu, Yaliang Zhao, and Qing Qin, Nonlinear resonance and envelope instability of intense beam in axial symmetric periodic channel, *Nucl. Instrum. Methods Phys. Res., Sect. A* **813**, 13 (2016).
- [45] M. Ikegami, Particle-core analysis of mismatched beams in a periodic focusing channel. *Phys. Rev. E* **59**, 2330 (1999).
- [46] S. M. Lund and S. R. Chawla, Space-charge transport limits of ion beams in periodic quadrupole focusing channels, *Nucl. Instrum. Methods Phys. Res., Sect. A* **561**, 203 (2006).
- [47] Ingo Hofmann, Adrian Oeftiger, and Oliver Boine-Frankenheim, Self-consistent long-term dynamics of space charge driven resonances in 2D, and 3D, *Phys. Rev. Accel. Beams* **24**, 024201 (2021).
- [48] Dong-O Jeon *et al.*, ‘Particle resonances’ domination over parametric instabilities, and their mitigation, in *Proceedings of the 68th ICFA Advanced Beam Dynamics Workshop on High-Intensity and High-Brightness Hadron Beams, HB2023 Workshop, CERN, Geneva* (CERN, Geneva, Switzerland, 2023).